

UC Santa Barbara

UC Santa Barbara Previously Published Works

Title

Trap-Assisted Auger-Meitner Recombination from First Principles

Permalink

<https://escholarship.org/uc/item/4q95595x>

Journal

Physical Review Letters, 131(5)

ISSN

0031-9007

Authors

Zhao, Fangzhou
Turiansky, Mark E
Alkauskas, Audrius
et al.

Publication Date

2023-08-04

DOI

10.1103/physrevlett.131.056402

Copyright Information

This work is made available under the terms of a Creative Commons Attribution-NonCommercial-NoDerivatives License, available at <https://creativecommons.org/licenses/by-nc-nd/4.0/>

Peer reviewed

Trap-Assisted Auger-Meitner Recombination from First Principles

Fangzhou Zhao^{1,*}, Mark E. Turiansky¹, Audrius Alkauskas^{2,‡}, and Chris G. Van de Walle^{1†}

¹ *Materials Department, University of California, Santa Barbara, CA 93106-5050, U.S.A. and*

² *Center for Physical Sciences and Technology (FTMC), Vilnius LT-10257, Lithuania* [‡]Deceased

(Dated: June 20, 2023)

Trap-assisted nonradiative recombination is known to limit the efficiency of optoelectronic devices, but the conventional multi-phonon emission (MPE) process fails to explain the observed loss in wide-band-gap materials. Here we highlight the role of trap-assisted Auger-Meitner (TAAM) recombination, and present a first-principles methodology to determine TAAM rates due to defects or impurities in semiconductors or insulators. We assess the impact on efficiency of light emitters in a recombination cycle that may include both TAAM and carrier capture via MPE. We apply the formalism to the technologically relevant case study of a calcium impurity in InGa_nN, where a Shockley-Read-Hall recombination cycle involving MPE alone cannot explain the experimentally observed nonradiative loss. We find that, for band gaps larger than 2.5 eV, the inclusion of TAAM results in recombination rates that are orders of magnitude larger than recombination rates based on MPE alone, demonstrating that TAAM can be a dominant nonradiative process in wide-band-gap materials. Our computational formalism is general and can be applied to the calculation of TAAM rates in any semiconducting or insulating material.

Auger-Meitner recombination [1–3] is an important nonradiative carrier recombination mechanism that has been widely invoked as a loss mechanism in optoelectronic devices [4]. The Auger-Meitner process involves an electron-hole recombination event with the energy transferred via Coulomb interaction to a third free carrier that is excited to a higher-energy state. The bulk Auger-Meitner process based on free carriers in the conduction bands (CBs) valence band (VBs) scales as the third power of the carrier density; it therefore dominates at high carrier densities and has been identified as responsible for the efficiency droop of solid-state light emitters [5–9]. In a trap-assisted Auger-Meitner (TAAM) process (Fig. 1), one of the carriers is localized on a point defect or impurity [10], and hence the recombination rate scales as the second power of the carrier density [11, 12]. This scaling allows the process to be distinguished from carrier capture by multiphonon emission (MPE) [12], which scales linearly with carrier density. TAAM recombination has occasionally been invoked as impacting the performance of semiconductor devices [13–16]; however, systematic studies are still lacking. Theoretical study has been based on analytic models [17] or focused on a specific scenario [18]. Here, we present a general first-principles formulation along with a computationally feasible implementation and an assessment of the impact on efficiency-limiting nonradiative recombination.

We illustrate the development of the formalism and the power of the approach by applying it to a relevant case study, namely a calcium impurity in InGa_nN, a key material for solid-state lighting. Unintentionally incorporated calcium was experimentally observed to severely impact the quantum efficiency of light-emitting diodes [19]. First-principles calculations of carrier capture via MPE [20], which is the most frequently discussed defect-assisted nonradiative recombination mechanism, indeed indicated that Ca acts as a strong Shockley-Read-Hall

(SRH) [21, 22] recombination center in InGa_nN with a band gap up to ~ 2.5 eV. For larger band gaps, however, Ca-assisted SRH rates become vanishingly small, because the capture rate via MPE decreases exponentially as the energy difference between the trap level and the band edge increases. Nonradiative SRH recombination based on MPE alone thus cannot explain the poor quantum efficiency in Ca-containing In_{0.1}Ga_{0.9}N layers with gaps close to 3 eV [19]. More generally, this rapid decrease in capture rate for defect levels farther from the band edges, combined with the fact that carrier capture from both VB and CB is necessary for a complete nonradiative recombination cycle, means that capture via MPE cannot explain defect-assisted efficiency loss in wider-band-gap semiconductors.

In this Letter, we show that TAAM recombination

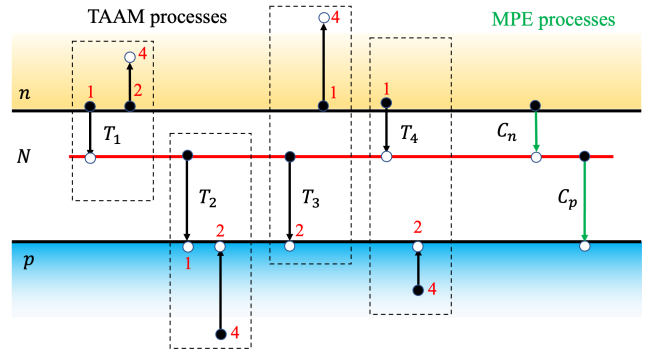


FIG. 1. Schematic diagram of the trap-assisted nonradiative recombination processes considered in this work: the four TAAM processes and the two MPE processes. The TAAM processes, labeled by T_1 , T_2 , T_3 , T_4 , are depicted in the dashed rectangles. Solid (hollow) circles denote electrons (holes). The arrows denote the electron transitions, and the red numbers denote the state numbers in Eqs. (1)-(4).

provides a compelling explanation for nonradiative loss in wide-band-gap semiconductors. Four distinct TAAM processes can occur at a trap with a single bound state (Fig. 1), characterized by the coefficients T_1 through T_4 [12]. For the capture of a free electron by the trap state, energy conservation is provided by exciting either a second free electron (process T_1) or a hole (T_4) to a higher-energy state. Similarly, hole capture at the trap can be accompanied by the excitation of another hole (T_2) or an electron (T_3).

Figure 1 also depicts the single-carrier processes, in which the energy resulting from electron or hole capture is released via MPE. Without loss of generality, we will consider the trap to be an acceptor, where the neutral

charge state (with density N^0) is the initial state for electron capture, and the negative charge state (with density N^-) the initial state for hole capture. The MPE rate for electron (hole) capture is linear in the carrier density n (p) and given by $R_n = C_n N^0 n$ ($R_p = C_p N^- p$) [23]. The electron (hole) capture coefficients C_n (C_p) have units cm^3s^{-1} . Recombination rates for the TAAM processes $R_{n,i}$ ($i = 1, 4$), $R_{p,i}$ ($i = 2, 3$) can similarly be expressed in terms of the coefficients T_i where n (p) denotes electron (hole) capture; these rates again scale with the trap density (N^0 or N^-) but they are *second order* in the carrier densities, since *two* free carriers are involved. These rates are calculated based on Fermi's golden rule and lead to the following expressions for the coefficients T_i [17]:

$$T_1 = \frac{R_{n,1}}{N^0 n^2} = \frac{2\pi}{\hbar} \frac{1}{n^2} \sum_{\mathbf{1} \in c, \mathbf{2} \in c, \mathbf{4} \in c} f_1 f_2 (1 - f_4) |M_{\mathbf{1}\mathbf{2}t\mathbf{4}}^1|^2 \delta(\epsilon_1 + \epsilon_2 - \epsilon_t - \epsilon_4), \quad (1)$$

$$T_2 = \frac{R_{p,2}}{N^- p^2} = \frac{2\pi}{\hbar} \frac{1}{p^2} \sum_{\mathbf{1} \in v, \mathbf{2} \in v, \mathbf{4} \in v} (1 - f_1)(1 - f_2) f_4 |M_{\mathbf{1}\mathbf{2}t\mathbf{4}}^2|^2 \delta(\epsilon_1 + \epsilon_2 - \epsilon_t - \epsilon_4), \quad (2)$$

$$T_3 = \frac{R_{p,3}}{N^- n p} = \frac{2\pi}{\hbar} \frac{1}{n p} \sum_{\mathbf{1} \in c, \mathbf{2} \in v, \mathbf{4} \in c} f_1 (1 - f_2)(1 - f_4) |M_{\mathbf{1}\mathbf{2}t\mathbf{4}}^3|^2 \delta(\epsilon_1 + \epsilon_t - \epsilon_2 - \epsilon_4), \quad (3)$$

$$T_4 = \frac{R_{n,4}}{N^0 n p} = \frac{2\pi}{\hbar} \frac{1}{n p} \sum_{\mathbf{1} \in c, \mathbf{2} \in v, \mathbf{4} \in v} f_1 (1 - f_2) f_4 |M_{\mathbf{1}\mathbf{2}t\mathbf{4}}^4|^2 \delta(\epsilon_1 + \epsilon_4 - \epsilon_t - \epsilon_2), \quad (4)$$

where c and v indicate the bulk states in the CB and VB continuum, and the trap-state level is labeled by t . f_j are free-carrier occupation numbers for the j -th carrier state according to Fermi-Dirac statistics. The δ function ensures energy conservation. The units of $R_{n/p,i}$ are $\text{cm}^{-3}\text{s}^{-1}$, and the units of T_i are cm^6s^{-1} . Vibrational broadening is included by replacing Eqs. (1)-(4) by a convolution with a normalized spectral function of electron-phonon interaction [24, 25].

The matrix elements $M_{\mathbf{1}\mathbf{2}t\mathbf{4}}^i$ for the four processes are given by:

$$M_{\mathbf{1}\mathbf{2}t\mathbf{4}}^1 = M_{\mathbf{1}\mathbf{2}t\mathbf{4}}^2 = \langle \mathbf{1}\mathbf{2} | \hat{W} | t\mathbf{4} \rangle - \langle \mathbf{1}\mathbf{2} | \hat{W} | \mathbf{4}t \rangle, \quad (5)$$

$$M_{\mathbf{1}\mathbf{2}t\mathbf{4}}^3 = \langle \mathbf{1}t | \hat{W} | \mathbf{4}\mathbf{2} \rangle - \langle \mathbf{1}t | \hat{W} | \mathbf{2}\mathbf{4} \rangle, \quad (6)$$

$$M_{\mathbf{1}\mathbf{2}t\mathbf{4}}^4 = \langle \mathbf{1}\mathbf{4} | \hat{W} | t\mathbf{2} \rangle - \langle \mathbf{1}\mathbf{4} | \hat{W} | \mathbf{2}t \rangle, \quad (7)$$

where each number or \mathbf{t} indicates the band indices and spin indices for a spin-polarized calculation, or the spinor wavefunction states in a noncollinear calculation. The matrix elements of the screened Coulomb interaction \hat{W} are given by

$$\langle \mathbf{1}\mathbf{2} | \hat{W} | t\mathbf{4} \rangle = \int \int d\mathbf{r}_1 d\mathbf{r}_2 \psi_1^*(\mathbf{r}_1) \psi_2^*(\mathbf{r}_2) W(\mathbf{r}_1, \mathbf{r}_2) \psi_t(\mathbf{r}_1) \psi_4(\mathbf{r}_2) \quad (8)$$

with \hat{W} approximated using a model dielectric function [26] [see Supplemental Material (SM), S1 [27]].

As already mentioned, a complete SRH recombination cycle [28] requires capture of both an electron and a hole. Here we address this complete cycle by taking into account that capture could occur through either MPE or TAAM. Assuming that $n = p$ (as is usually the case in light emitters due to charge neutrality), the total trap-assisted nonradiative recombination rate is then given by (see SM, S2 [27]):

$$R_{tot} = N \frac{(T_1 + T_4 + C_n/n)(T_2 + T_3 + C_p/n)}{T_1 + T_2 + T_3 + T_4 + (C_n + C_p)/n} n^2 \quad (9)$$

where $N = N^0 + N^-$ is the total density of traps. We note that this rate is second order in n at high carrier density, but still linear (as in the ‘‘usual’’ SRH recombination cycle) if the TAAM coefficients are small and the carrier density is low.

Our quantitative calculations of TAAM coefficients are based on first-principles density functional theory using the QUANTUM ESPRESSO (QE) package [29]. To obtain accurate results for defects and impurities [30] we use the hybrid functional of Heyd-Scuseria-Ernzerhof (HSE) [31]. For our case study of Ca in GaN we use a 120-Ry energy cutoff, and the fraction of screened Fock exchange α in the HSE functional is set to 0.33, which results in a GaN band gap of 3.55 eV, in agreement with experiment [32]. Our calculations use norm-conserving pseudopotentials,

and we have tested that the Ga d states can be treated as part of the core; details about this and other tests of the accuracy of our calculations are included in SM, S3 [27].

Spin polarization is included. Energetics are calculated in a 96-atom supercell with a $2 \times 2 \times 2$ Monkhorst-Pack k -point grid. Finite-size corrections for charged systems are applied [33, 34]. For the evaluation of TAAM coefficients, we used the Γ point in fully relaxed 96-, 360-, and 768-atom supercells (see SM, S4 [27]).

Figure 2(a) shows the calculated formation energy of the substitutional Ca_{Ga} impurity, which was found to be relevant for nonradiative recombination [20]. Ca_{Ga} acts as a deep acceptor with a $(0/-)$ level ~ 1.01 eV above the valence-band maximum (VBM). The inset in Fig. 2(a) shows the Kohn-Sham wavefunction of the single trap state in the gap in the minority-spin channel: it is a p -like orbital localized at a nitrogen atom adjacent to the Ca impurity atom.

Electron-phonon interactions, which we need for evaluation of the MPE [35] as well as to include vibrational broadening [36] in the TAAM processes are evaluated based on a one-dimensional configuration coordinate diagram [Fig. 2(b)] [37], which is justified in the case of strong electron-phonon coupling [24]. The transition energy for electron capture ΔE^n , also known as the zero-phonon line, is the energy difference between the conduction-band minimum (CBM) and the $(0/-)$ transition level (and *mutatis mutandis* for hole capture ΔE^p). The Franck-Condon energies are $E_{FC}^e = 0.55$ eV for electron capture and $E_{FC}^h = 0.50$ eV for hole capture, and the Huang-Rhys factors are $S^e = \frac{E_{FC}^e}{\hbar\Omega_e} \approx 15$ and $S^h = \frac{E_{FC}^h}{\hbar\Omega_g} \approx 16$.

In the case of strong electron-phonon coupling (large Huang-Rhys factors), the electron-phonon spectral func-

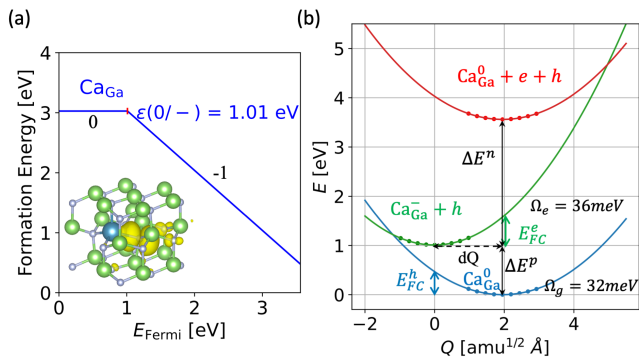


FIG. 2. (a) Formation energy vs. Fermi level for Ca_{Ga} in neutral and negative charge states under Ga-rich conditions. The atomic geometry and trap-state wavefunction of neutral Ca_{Ga} are illustrated in the inset. (b) Configuration coordinate diagram illustrating electron and hole capture processes. The symbols denote calculated values; the lines are parabolic fits.

tion is well approximated by a Gaussian with a variance σ determined based on the S and Ω parameters [37, 38] (See SM, S6 [27]). We include phonon assistance in the TAAM coefficient for the T_1 process by replacing $\delta(\epsilon_1 + \epsilon_2 - \epsilon_t - \epsilon_4)$ by a Gaussian function g centered at $[\epsilon_1 + \epsilon_2 - \epsilon(0/-) - \epsilon_4 - E_{FC}^e]$. Similar expressions apply to the other processes. The energy of the KS state ϵ_t is replaced by $[\epsilon(0/-) + E_{FC}^e]$ to reflect that the vertical transition energy [Fig. 2(b)] released by the first carrier is transferred to the second carrier. σ is found to be close to 0.22 eV for all processes.

Particular attention needs to be paid to the summation over the 4^{th} bulk state in Eqs. (1)-(4). This state is sparsely sampled in our supercell calculations in cases T_1 and T_3 due to the highly dispersive nature of the lowest CB [as shown by sampled Kohn-Sham states in the CB continuum illustrated in Fig. 3(a)]. Sampling of the VB states (cases T_2 and T_4) is far easier thanks to lower dispersion and zone folding in the supercell. For T_1 and T_3 , we therefore perform the summation over the 4^{th} CB state in a more physical way by a continuous integration according to the bulk CB density of states $D(\epsilon)$:

$$T_1 = \frac{2\pi}{\hbar} \frac{1}{n^2} \sum_{1 \in c, 2 \in c} \int_{CBM}^{\infty} d\epsilon_4 D(\epsilon_4) f_1 f_2 (1 - f_4(\epsilon_4)) \times \overline{|M_{12t4}^1|^2} g[\epsilon_1 + \epsilon_2 - \epsilon(0/-) - \epsilon_4 - E_{FC}^e]. \quad (10)$$

The use of an average value $\overline{|M_{12t4}^1|^2}$ is justified because the orbital character of the CB, and hence the matrix element, varies little over the relevant energy range (see SM, S5 [27]). The upper bound of the integration is chosen to fully include the (vibrationally broadened) energy-conserving transition. When calculating TAAM coefficients for a material with a highly dispersive VB the same technique should be applied to T_2 and T_4 .

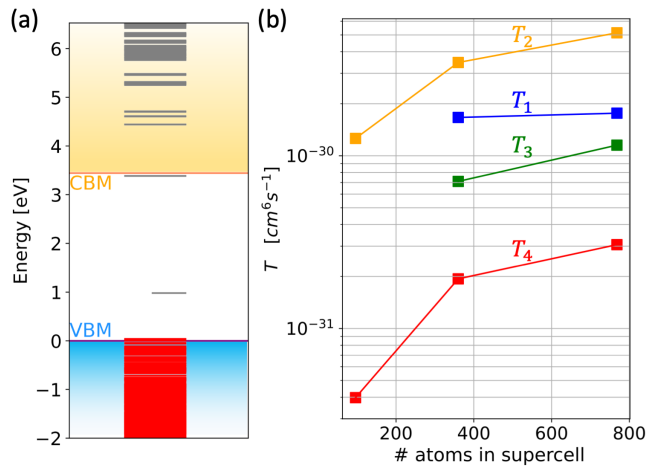


FIG. 3. (a) Kohn-Sham states for Ca_{Ga} in GaN calculated in a 768-atom supercell. (b) Calculated TAAM coefficients as a function of supercell size.

Figure 3(b) shows our calculated values for the T_i coefficients using 96-, 360-, and 768-atom supercells at $T=390$ K. Values for T_1 and T_3 in the 96-atom supercell are not included due to the sparse sampling of CB states. Comparing the 360- and 768- atom supercell calculations, the coefficients are converged to within a factor of two, a satisfactory level of accuracy. Extensive checks indicated that the T_i coefficients depend only weakly on the position of the trap-state level in the band gap or on the value of the broadening parameter (See SM, S6 and S7 [27]).

We now investigate the TAAM coefficients and the total nonradiative recombination rate in InGaN alloys. Since explicit alloy calculations are prohibitively expensive, we use interpolation procedures similar to previous work on bulk Auger-Meitner [7, 9] and SRH recombination [20, 39]. VBM and CBM positions in $\text{In}_x\text{Ga}_{1-x}\text{N}$ for $x < 0.5$ are taken from Refs. 39 and 40 and the (0/-) transition level is interpolated based on explicit calculations at discrete values of x [20] following the procedure outlined in Ref. 39 and 40. T_i coefficients as a function of $\text{In}_x\text{Ga}_{1-x}\text{N}$ gap are then calculated using the 360-atom supercell based on wavefunctions for Ca_{Ga} in GaN but with the band edges and trap-state level rigidly shifted as specified above.

Figure 4(a) shows that all of the T_i coefficients are on the order of 10^{-30} cm^6s^{-1} . The T_2 and T_3 coefficients are almost independent of $\text{In}_x\text{Ga}_{1-x}\text{N}$ gap since they are based on hole capture to the trap-state level, and the (0/-) level largely tracks the VBM [20]. In contrast, T_1 and T_4 show larger variations, since the position of the (0/-) level relative to the CBM changes from 2.5 eV in GaN to 0.7 eV in $\text{In}_{0.5}\text{Ga}_{0.5}\text{N}$ [20]. For T_1 , a larger energy difference allows electron excitations to higher-lying CB states (Fig. 1) where the density of CB states is larger. The variation trend is different for T_4 , which involves excitation of a hole into the VB (see SM, S6 [27]).

Still, the variation of the T_1 and T_4 coefficients with band gap is relatively minor when compared to the huge change in the MPE capture coefficient C_n [Fig. 4(b)] [41]. This is because, in a semiclassical picture, MPE capture depends exponentially on a barrier height that increases linearly with the energy difference between the trap level and the CBM [12, 42]; no such activated behavior occurs in TAAM, where final states in the continuum are readily available at any energy. The absence of activated behavior, and of the need for momentum conservation, also explain the TAAM coefficients' very weak dependence on temperature, as we have verified by explicit calculations. This implies that TAAM recombination will persist as a loss mechanism even at low temperatures. [43]

These results now allow us to determine the total trap-assisted nonradiative recombination rate due to Ca_{Ga} in InGaN as a function of InGaN band gap. We use the $N = 10^{18}$ cm^{-3} Ca concentration from the experimental study [19] and a typical operating carrier density of $n = 10^{18}$

cm^{-3} . Figure 4 compares the total recombination rate R_{tot} with the rate R_{MPE} assuming only MPE processes [obtained from Eq. (9) by setting all T_i to zero]. For band gaps less than ~ 2.5 eV the rate is dominated by MPE capture; however, due to the increasing energy difference with the CBM, the MPE-assisted electron capture rate rapidly decreases with band gap. Around 2.5 eV TAAM becomes the dominant electron capture process, and due to its relative insensitivity to band gap [Fig. 4(a)] the overall R_{tot} remains relatively constant (or even slightly increases) as a function of band gap.

For $\text{In}_{0.1}\text{Ga}_{0.9}\text{N}$ (as used in Ref. [19]) the gap is ~ 3.0 eV and the calculated R_{tot} is 2×10^{24} $\text{cm}^{-3}\text{s}^{-1}$, 11 orders of magnitude larger than the rate based on the MPE process alone. To put this in perspective, the calculated radiative recombination rate for $\text{In}_{0.1}\text{Ga}_{0.9}\text{N}$ is about $4 \times 10^{25}\text{cm}^{-3}\text{s}^{-1}$ [44], so, to within the calculation error bars,

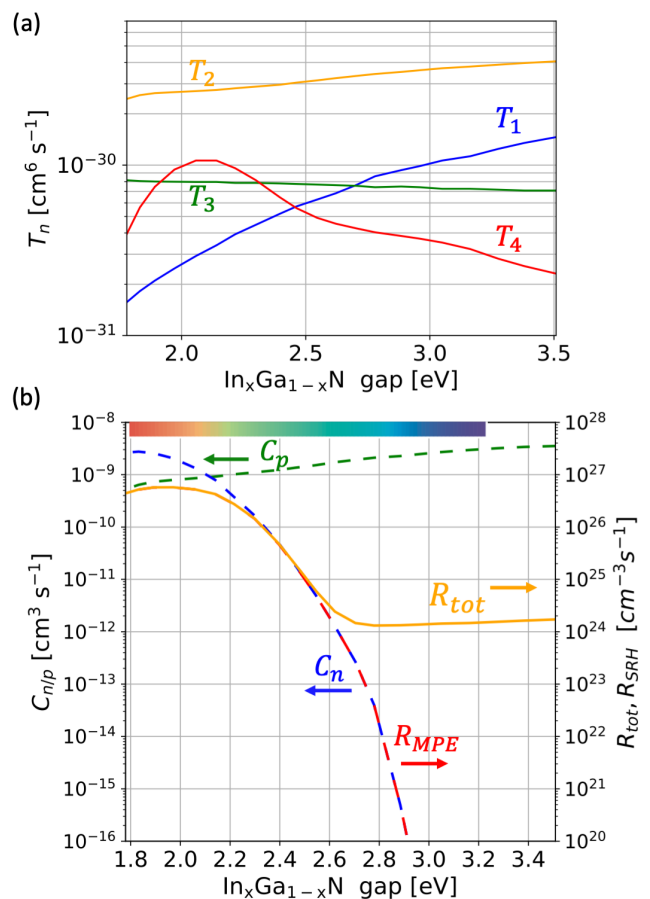


FIG. 4. (a) Calculated TAAM coefficients for Ca_{Ga} as a function of $\text{In}_x\text{Ga}_{1-x}\text{N}$ band gap. (b) Calculated MPE capture coefficients C_n and C_p (dashed lines, left axis), as well as the total trap-assisted nonradiative recombination rate (right axis) calculated at $T=390$ K with $N = 10^{18}$ cm^{-3} and $n = 10^{18}$ cm^{-3} . R_{tot} (orange curve) includes the two MPE processes plus the four TAAM processes [Eq. (9)], while R_{MPE} (red dashed curve) includes only the MPE processes.

nonradiative recombination due to Ca can significantly impact efficiency, as experimentally observed [19]—but it is essential to include TAAM processes.

Based on our calculated numbers, at band gaps where $C_n \ll n(T_1 + T_4)$ the expression for R_{tot} can be approximated as $R_{tot} \approx N(T_1 + T_4)n^2$. We note that the n^2 dependence is the same as that of the *radiative* recombination rate, which may explain why TAAM processes have generally been overlooked in studies of internal quantum efficiency as a function of carrier density. In their very careful analysis, Espenlaub *et al.* [15] indeed observed the presence of a nonradiative recombination mechanism scaling as n^2 ; and Myers *et al.* [16] found evidence for hot electrons in the conduction band, consistent with our calculations that show the T_1 electron capture process to be dominant.

Unlike MPE rates, which decrease exponentially with band gap [12, 42], TAAM processes are not suppressed in large-gap materials because they are based on Coulomb interactions that can occur at any energy and for which final states are always available. The interaction matrix elements are related to wavefunction overlap between the defect states and bulk states, and it is reasonable to expect that for many defects in other materials they can be of the same magnitude as evaluated here for Ca_{Ga} in GaN. Thus, TAAM recombination is not a material-specific process. As a result, inclusion of the TAAM-assisted processes can account for the observed nonradiative recombination rate in wider-band-gap materials, where rates due to MPE alone become negligibly low.

In conclusion, we have developed a first-principles formalism to calculate trap-assisted Auger-Meitner recombination rates. For our test case of Ca_{Ga} impurities in InGaN, the results show that including TAAM processes is essential to explain the observed trap-assisted nonradiative recombination rates in materials with band gaps greater than ~ 2.5 eV. Our formalism is general and can be applied to study TAAM recombination in any semiconductor or insulator. The approach provides insight into the physics of nonradiative recombination processes and elucidates why TAAM processes are key to describing defect-assisted recombination in wider-band-gap materials, where MPE alone fails to explain efficiency loss.

We dedicate this work to the memory of Audrius Alkauskas, an outstanding scientist, generous colleague, and caring friend. We acknowledge fruitful discussions with E. Kioupakis. This study was supported by the US Department of Energy (DOE), Office of Science, Basic Energy Sciences (BES) under Award No. DE-SC0010689. F.Z. acknowledges support from the California NanoSystems Institute for an Elings Prize Fellowship. M.E.T. was supported by the National Science Foundation (NSF) through Enabling Quantum Leap: Convergent Accelerated Discovery Foundries for Quantum Materials Science, Engineering and Information (Q-AMASE-i) Award No. DMR-1906325 and by the Office of Naval Research,

Award No. N00014-22-1-2808 (Vannevar Bush Faculty Fellowship). Computational resources were provided by the National Energy Research Scientific Computing Center, a DOE Office of Science User Facility supported by the Office of Science of the DOE under Contract No. DE-AC02-05CH11231.

* fangzhouzhao@ucsb.edu

† vandewalle@mrl.ucsb.edu

- [1] L. Meitner, *Z. Phys.* **9**, 131 (1922).
- [2] P. Auger, *C. R. Acad. Sci.(F)* **177**, 169 (1923).
- [3] We adopt the term ‘‘Auger-Meitner’’ effect, in recognition of the fact that the atomic emission process was independently discovered by Meitner in 1922 [1] and by Auger in 1923 [2]; see D. Matsakis, A. Coster, B. Laster, and R. Sime, *Phys. Today* **72**, 10 (2019).
- [4] E. F. Schubert, *Light-emitting diodes cambridge university press* (Cambridge University Press, Cambridge, 2006).
- [5] N. Gardner, G. Müller, Y. Shen, G. Chen, S. Watanabe, W. Götz, and M. Krames, *Appl. Phys. Lett.* **91**, 243506 (2007).
- [6] Y. Shen, G. Mueller, S. Watanabe, N. Gardner, A. Munkholm, and M. Krames, *Appl. Phys. Lett.* **91**, 141101 (2007).
- [7] E. Kioupakis, P. Rinke, K. T. Delaney, and C. G. Van de Walle, *Appl. Phys. Lett.* **98**, 161107 (2011).
- [8] J. Iveland, L. Martinelli, J. Peretti, J. S. Speck, and C. Weisbuch, *Phys. Rev. Lett.* **110**, 177406 (2013).
- [9] E. Kioupakis, D. Steiauf, P. Rinke, K. T. Delaney, and C. G. Van de Walle, *Phys. Rev. B* **92**, 035207 (2015).
- [10] L. Bess, *Phys. Rev.* **111**, 129 (1958).
- [11] P. Landsberg, C. Rhys-Roberts, and P. Lal, *Proc. Phys. Soc. (1958-1967)* **84**, 915 (1964).
- [12] V. N. Abakumov, V. I. Perel, and I. N. Yassievich, *Nonradiative recombination in semiconductors* (Elsevier, North-Holland, Amsterdam, 1991).
- [13] A. Hangleiter, *Phys. Rev. Lett.* **55**, 2976 (1985).
- [14] A. W. Cohn, A. M. Schimpf, C. E. Gunthardt, and D. R. Gamelin, *Nano Lett.* **13**, 1810 (2013).
- [15] A. C. Espenlaub, D. J. Myers, E. C. Young, S. Marcinkevičius, C. Weisbuch, and J. S. Speck, *J. Appl. Phys.* **126**, 184502 (2019).
- [16] D. J. Myers, A. C. Espenlaub, K. Gelzinyte, E. C. Young, L. Martinelli, J. Peretti, C. Weisbuch, and J. S. Speck, *Appl. Phys. Lett.* **116**, 091102 (2020).
- [17] A. Haug, *Phys. Status Solidi (b)* **97**, 481 (1980).
- [18] P. Siyushev, H. Pinto, M. Vörös, A. Gali, F. Jelezko, and J. Wrachtrup, *Phys. Rev. Lett.* **110**, 167402 (2013).
- [19] E. Young, N. Grandjean, T. Mates, and J. Speck, *Appl. Phys. Lett.* **109**, 212103 (2016).
- [20] J.-X. Shen, D. Wickramaratne, C. E. Dreyer, A. Alkauskas, E. Young, J. S. Speck, and C. G. Van de Walle, *Appl. Phys. Express* **10**, 021001 (2017).
- [21] W. Shockley and W. Read Jr, *Phys. Rev.* **87**, 835 (1952).
- [22] R. N. Hall, *Phys. Rev.* **87**, 387 (1952).
- [23] A. Alkauskas, Q. Yan, and C. G. Van de Walle, *Phys. Rev. B* **90**, 075202 (2014).
- [24] A. Alkauskas, J. L. Lyons, D. Steiauf, and C. G. Van de Walle, *Phys. Rev. Lett.* **109**, 267401 (2012).

- [25] L. Razinkovas, M. Maciaszek, F. Reinhard, M. W. Doherty, and A. Alkauskas, *Phys. Rev. B* **104**, 235301 (2021).
- [26] G. Cappellini, R. Del Sole, L. Reining, and F. Bechstedt, *Phys. Rev. B* **47**, 9892 (1993).
- [27] See Supplemental Material [url] (which includes Refs. [9, 20, 26, 29, 32, 37, 38, 45-53]) for S1: Screened Coulomb interaction matrix elements in TAAM Auger coefficients calculations; S2: Total trap-assisted nonradiative recombination rate including TAAM and MPE processes; S3: Details of density functional theory calculations; S4: Supercells used in the TAAM calculations; S5: Density-of-states integration method for the 4th bulk state in the calculation of T_i coefficients; S6: TAAM coefficients as function of trap-state level position and broadening parameter; and S7: Accuracy analysis of TAAM coefficients calculation.
- [28] In the original work [21, 22] Shockley, Read, and Hall only considered processes with rates proportional to the carrier density, but since "SRH recombination" has become almost synonymous with "trap-assisted recombination" we suggest that TAAM process should be included..
- [29] P. Giannozzi, S. Baroni, N. Bonini, M. Calandra, R. Car, C. Cavazzoni, D. Ceresoli, G. L. Chiarotti, M. Cococcioni, I. Dabo, *et al.*, *J. Phys. Condens. Matter* **21**, 395502 (2009).
- [30] C. Freysoldt, B. Grabowski, T. Hickel, J. Neugebauer, G. Kresse, A. Janotti, and C. G. Van de Walle, *Rev. Mod. Phys.* **86**, 253 (2014).
- [31] J. Heyd, G. E. Scuseria, and M. Ernzerhof, *J. Chem. Phys.* **118**, 8207 (2003); *ibid.* **124**, 219906 (2006), (erratum).
- [32] O. Madelung, *Semiconductors: Data Handbook, 3rd ed.* (Springer, Berlin, 2004).
- [33] C. Freysoldt, J. Neugebauer, and C. G. Van de Walle, *Phys. Rev. Lett.* **102**, 016402 (2009).
- [34] C. Freysoldt, J. Neugebauer, and C. G. Van de Walle, *Phys. Status Solidi (b)* **248**, 1067 (2011).
- [35] M. E. Turiansky, A. Alkauskas, M. Engel, G. Kresse, D. Wickramaratne, J.-X. Shen, C. E. Dreyer, and C. G. Van de Walle, *Comput. Phys. Commun.* **267**, 108056 (2021).
- [36] A. Stoneham, *Rep. Prog. Phys.* **44**, 1251 (1981).
- [37] A. Alkauskas, M. D. McCluskey, and C. G. Van de Walle, *J. Appl. Phys.* **119**, 181101 (2016).
- [38] Y. Jia, S. Poncé, A. Miglio, M. Mikami, and X. Gonze, *J. Lumin.* **224**, 117258 (2020).
- [39] C. E. Dreyer, A. Alkauskas, J. L. Lyons, J. S. Speck, and C. G. Van de Walle, *Appl. Phys. Lett.* **108**, 141101 (2016).
- [40] P. G. Moses and C. G. Van de Walle, *Appl. Phys. Lett.* **96**, 021908 (2010).
- [41] The MPE capture coefficients C_n and C_p are calculated using the formalism of Ref. 23 as implemented in the Nonrad code [35]; the values are consistent with previous work [20].
- [42] A. Alkauskas, C. E. Dreyer, J. L. Lyons, and C. G. Van de Walle, *Phys. Rev. B* **93**, 201304 (2016).
- [43] A. Hangleiter, *Phys. Rev. B* **35**, 9149 (1987).
- [44] E. Kioupakis, Q. Yan, D. Steiauf, and C. G. Van de Walle, *New J. Phys.* **15**, 125006 (2013).
- [45] D. Manchon Jr, A. Barker Jr, P. Dean, and R. Zetterstrom, *Solid State Commun.* **8**, 1227 (1970).
- [46] A. Barker Jr and M. Ilegems, *Phys. Rev. B* **7**, 743 (1973).
- [47] G. Kresse and J. Furthmüller, *Phys. Rev. B* **54**, 11169 (1996).
- [48] G. Kresse and J. Furthmüller, *Comput. Mater. Sci* **6**, 15 (1996).
- [49] P. E. Blöchl, *Phys. Rev. B* **50**, 17953 (1994).
- [50] M. Fuchs and M. Scheffler, *Comput. Phys. Commun.* **119**, 67 (1999).
- [51] J. L. Lyons and C. G. Van de Walle, *NPJ Comput. Mater.* **3**, 12 (2017).
- [52] J. L. Lyons, D. Wickramaratne, and C. G. Van de Walle, *J. Appl. Phys.* **129**, 111101 (2021).
- [53] I. Diallo and D. Demchenko, *Phys. Rev. Appl.* **6**, 064002 (2016).